Non-Enzymatic and Highly Sensitive Lactose Detection Utilizing Graphene Field-Effect Transistors

Eric Danielson*[1], Mirco Dindo[2], Alexander J. Porkovich[1], Pawan Kumar[1], Zhenwei Wang[1], Prashant Jain[3], Trimbak Mete[3], Zakaria Ziadi[1], Raghavendra Kikkeri[3], Paola Laurino[2], Mukhles Sowwan[1]

[1]Nanoparticles by Design Unit, Okinawa Institute of Science and Technology (OIST) Graduate University, 1919-1 Tancha, Onna-Son, Okinawa 904-0495, Japan

[2]Protein Engineering and Evolution Unit, Okinawa Institute of Science and Technology (OIST) Graduate University, 1919-1 Tancha, Onna-Son, Okinawa 904-0495, Japan

[3]Indian Institute of Science Education and Research, Dr. Homi Bhabha Road, Pune, 411008, India.

Keywords

Lactose biosensor; field effect transistor; lectin; graphene; gold nanoparticles

© 2021. This manuscript version is made available under the CC-BY-NC-ND 4.0 license
http://creativecommons.org/licenses/by-nc-nd/4.0/

Abstract

Field-effect transistor (FET) biosensors based on low-dimensional materials are capable of highly sensitive and specific label-free detection of various analytes. In this work, a FET biosensor based on graphene decorated with gold nanoparticles (Au NPs) was fabricated for lactose detection in a liquid-gate measurement configuration. This graphene device is functionalized with a carbohydrate recognition domain (CRD) of the human galectin-3 (hGal-3) protein to detect the presence of lactose from the donor effect of lectin – glycan affinity binding on the graphene. Although the detection of lactose is important because of its ubiquitous presence in food and for disease related applications (lactose intolerance condition), in this work we exploit the lectin/carbohydrate interaction to develop a device that in principle could specifically detect very low concentrations of any carbohydrate. The biosensor achieved an effective response to lactose concentrations over a dynamic range from 1 fM to 1 pM (10^{-15} to 10^{-12} mol L^{-1}) with a detection limit of 200 aM, a significant enhancement over previous electrochemical graphene devices. The FET sensor response is also specific to lactose at aM concentrations, indicating the potential of a combined lectin and graphene FET (G-FET) sensor to detect carbohydrates at high sensitivity and specificity for disease diagnosis.

© 2021. This manuscript version is made available under the CC-BY-NC-ND 4.0 license
http://creativecommons.org/licenses/by-nc-nd/4.0/

1. Introduction

Graphene field-effect transistors (G-FETs) have been employed as ultrasensitive, label-free sensors for the electrical detection of a variety of analytes (Justino et al., 2017; Peña-Bahamonde et al., 2018). By functionalizing the graphene surface with a biological recognition element, the sensor response is engineered to be highly specific (Matsumoto et al., 2014; Fu et al., 2017). Graphene is an attractive nanomaterial for FET biosensors due to its high conductivity and ease of functionalization (Suvarnaphaet et al., 2017). Every atom in a graphene sheet is in contact with the solution environment and responds to external electrostatic fluctuations, making G-FETs highly sensitive with limits of detection (LoD) for proteins or DNA at attomolar to femtomolar concentrations (Kim et al., 2013; Cai et al., 2015; Lei et al., 2017; Campos et al., 2019).

G-FETs have also been employed as sensors for glucose (Viswanathan et al., 2015), fructose (Zhao et al., 2019), and lactose (Nguyen et al., 2016). In these electrochemical biosensors, the sensor response is generated from a change in hydrogen peroxide upon oxidation of the target carbohydrate, catalyzed with enzymes or metal NPs attached to the graphene. Despite recent achievements in G-FET carbohydrate biosensor development, their LoD has been limited to nanomolar or micromolar levels (Liao et al., 2013; Cagang et al., 2016).

G-FET carbohydrate biosensor development could take advantage of the natural occurring proteins that bind specific carbohydrates, namely lectins. Lectins recognize the terminal or penultimate sugar residue, their glycosidic linkages (α or β) and possibly associated functional groups (e.g. acetyl). While few lectins bind glycans with medically useful affinity, i.e. at least nanomolar affinity, a vast majority bind with low affinity in the micromolar range (Varki et al., 2017). This is primarily because the non-covalent lectin-glycan interactions are mediated by weak H-bonds or van der Waals contacts. However, nature compensates this handicap with multivalent interactions involving oligomeric carbohydrate recognition

© 2021. This manuscript version is made available under the CC-BY-NC-ND 4.0 license
http://creativecommons.org/licenses/by-nc-nd/4.0/

domains (CRDs) that simultaneously interact with several glycans on the same cell surface, thus leading to an avidity effect and consequently to tight and specific binding (Drickamer, 1995; Lee et al., 1995; Kiessling et al., 1996). The paramount challenge is to detect a very low concentration of glycans (nM concentration or even lower) with a single lectin. This task can be achieved by exploiting the advantages of a G-FET sensor.

Herein, we choose human galectin 3 (hGal-3) among all the natural lectins since hGal-3 is very well studied and extensive structural information is currently available. This structural information is essential to plan the mutations for the functionalization of the G-FET device. The C-terminal CRD of hGal-3, which shows close structural homology between the galectins, specifically binds to β-galactoside residues. Among the β-galactosides, hGal-3 binds the disaccharide lactose with a dissociation constant in the range of 150-250 μM (Saraboji et al., 2012). Lactose is composed of galactose and glucose subunits and is a very important dietary disaccharide found naturally in the milk of most mammals.

A system that combines a lectin such as Gal-3 and a G-FET sensor will be a powerful tool to recognize carbohydrates with high specificity and sensitivity. In this work, we choose to test our biosensor for lactose which is the minimum glycan unit that Gal-3 can bind with lowest affinity. This choice allows us to understand how effective the system is at detecting low affinity binders.

© 2021. This manuscript version is made available under the CC-BY-NC-ND 4.0 license
http://creativecommons.org/licenses/by-nc-nd/4.0/

2. Materials and Methods

2.1 Graphene FET Fabrication

Monolayer graphene was synthesized using a chemical vapor deposition (CVD) system, transferred to $Si:SiO_2$ substrates using a lamination procedure described in (Shivayogimath et al., 2019), then patterned into G-FETs using photolithography and metal e-beam evaporation (**Section S1**). The graphene was confirmed to be a monolayer thin film using Raman spectroscopy (**Fig. S1**).

G-FET devices were decorated with gold nanoparticles (Au NPs) using a direct-current (DC) magnetron-sputtering inert-gas aggregation system (**Fig. S2a**) described in previous publications (Porkovich et al., 2019) and in **Section S2**. A PDMS solution well was attached to the G-FET to protect the source and drain electrodes during liquid-gate measurements. Liquid PDMS was placed on the underside of a hollow PDMS cylinder, then cured at 90 °C for 1 hour for good adhesion to the FET surface. The solution well enclosed three G-FETs, each with an area of 1 mm^2. A schematic of a completed enclosed Au NP decorated G-FET is shown in **Fig. 1a**. The mechanism of analyte detection using liquid gate measurements of a functionalized G-FET is discussed in **Section S1**.

© 2021. This manuscript version is made available under the CC-BY-NC-ND 4.0 license
http://creativecommons.org/licenses/by-nc-nd/4.0/

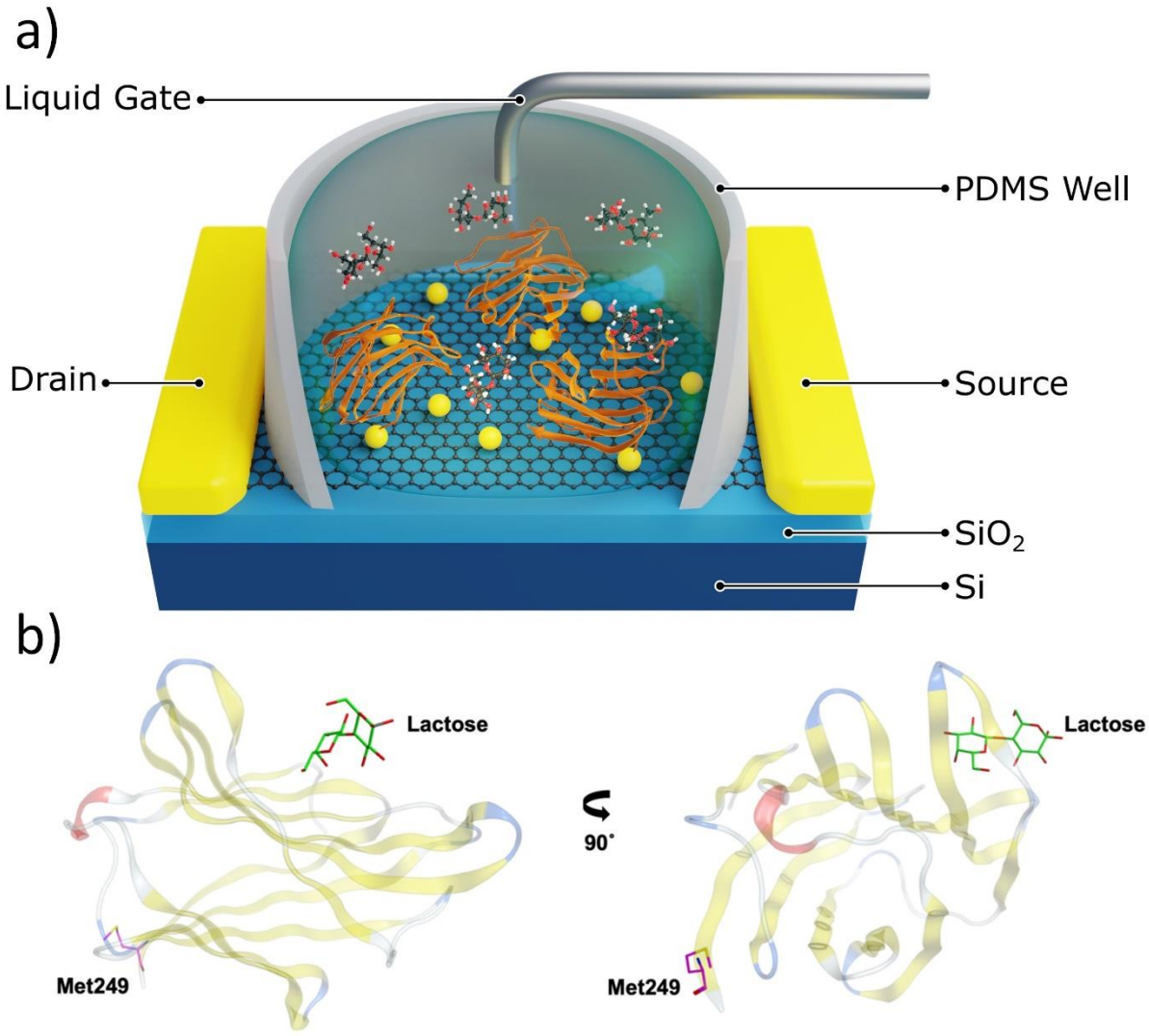

Fig. 1: G-FET Sensor & Protein Schematics. (a) Schematic diagram of a liquid-gated graphene FET biosensor. **(b)** Crystal structure of hGal-3 CRD with lactose PDB ID: 2NN8 (Collins et al., 2007). The Met249 residue is highlighted in violet and the lactose in green.

2.2 CRD hGal-3 Cloning and mutagenesis; CRD hGal-3 and hGal-3 M249C expression and purification

Lactose was obtained from Sigma Aldrich. Isopropyl-β-d-thiogalactopyranoside (IPTG), Protease Inhibitor Cocktail and PBS buffer were obtained from Nacalai Tesque, Kyoto, Japan. All other chemicals were of the highest grade commercially available. The protein cloning, site-directed mutagenesis, expression and

© 2021. This manuscript version is made available under the CC-BY-NC-ND 4.0 license
http://creativecommons.org/licenses/by-nc-nd/4.0/

purification procedures of CRD domain of hGal-3 and the mutant M249C are described in detail in the Supporting Information, **Section S3**. The purity of the proteins was verified by SDS-PAGE. The structure of CRD of hGal-3 with the residue 249 highlighted in blue is shown in **Fig. 1b** and the SDS-PAGE results of the CRD WT and M249C are shown in **Fig. S3**.

2.3 CRD hGal-3 and hGal-3 M249C mutant characterization

Circular dichroism spectra were obtained using a Jasco J-820 spectropolarimeter (Jasco, Tokyo, Japan) with a thermostatically controlled compartment at 25 °C. Far-UV measurements were recorded over the 190-260 nm range at a scanning speed of 100 nm/min subjected to fivefold signal averaging, at a protein concentration of 10 µM using a path length of 0.1 cm. The measurements were performed in 0.01x PBS pH 7.4 in triplicate.

Isothermal titration calorimetry (ITC) measurements were performed using MicroCal PEAQ-ITC (Malvern). The protein (CRD domain or the mutant M249C) was added in the cell at the concentration of 25-30 µM while the ligand (lactose 2 mM) was titrated from the syringe. All the experiments have been performed in 0.01x PBS pH 7.4 in triplicate. The cell temperature was maintained at 25 °C. Lactose was separately injected into 0.01x PBS pH 7.4 to verify that the heat of dilution was not significant. Fitting of the resulting curves from the experimental data have been done with the software provided by Microcal (Malvern).

2.4 Observation of Au NP – Protein binding

Atomic force microscopy (AFM) was used to measure the Au NPs density on graphene devices and measure the change in surface topography after protein binding. AFM measurements were performed on a conventional Multimode 8 scanning probe microscope (Bruker, USA) in PeakForce tapping mode. The

© 2021. This manuscript version is made available under the CC-BY-NC-ND 4.0 license
http://creativecommons.org/licenses/by-nc-nd/4.0/

high-resolution AFM probe (ScanAsyst-Air) from Bruker with nominal tip radius ~2 nm, resonant frequency 70 kHz, and low spring constant 0.4 N/m were used for all AFM measurements. High resolution (512 by 512 pixels) AFM images were captured at a scan rate of 0.5 Hz and further processed by using the Nanoscope Analysis software (Ver 9).

Protein immobilization on the Au NP decorated graphene sheet was examined using fluorescent microscopy. CDR hGal-3 M249C mutant was labeled with the probe Alexa Fluor 488 nm following the manufacturer protocol (Microscale Protein labeling Alexa Fluor 488 dye, Thermofisher Scientific, Massachusetts, USA). A 40 µL drop of 10 µM protein solution was placed on the graphene sheet for 2 hours at room temperature, before rinsing with 1x PBS and DI water to remove unbound proteins. Bare and Au NP decorated graphene sheets were exposed to the protein solution and imaged under a fluorescent confocal microscope (Zeiss LSM 510). The maximum excitation and emission wavelengths of the fluorescent tag are 490 and 525 nm, respectively. Images and intensity profiles were obtained using ImageJ (NIH).

2.5 Electrical Measurements

The transfer characteristics of the liquid-gated G-FETs were measured using a semiconductor parameter analyzer (Keithley 4200-SCS-A) under a constant drain to source (V_{ds}) bias of 0.1 V. A silver wire (1 mm diameter) was used as the liquid gate electrode (Chen et al., 2013). The G-FET was functionalized by placing a 40 µL drop of 10 µM protein solution in the solution well for 2 hours at room temperature. The device was rinsed with 1x PBS and DI water to remove unbound proteins. Before carbohydrate detection experiments, the graphene surface was passivated by incubating a 5 µM solution of bovine serum albumin (BSA) in DI water for 1 hour. The schematic in **Fig. 1a** shows the measurement configuration, with the

© 2021. This manuscript version is made available under the CC-BY-NC-ND 4.0 license
http://creativecommons.org/licenses/by-nc-nd/4.0/

reference electrode and the monolayer graphene functionalized with M249C CRD exposed to a lactose solution.

3. Results

3.1 Au NP Decorated Graphene and Protein Characterization

From AFM images taken after Au NP decoration of graphene sheets using the magnetron sputtering system (**Fig. 2a**), we see an even distribution of Au NPs is present over the monolayer graphene. Root-mean-squared (RMS) roughness was ~ 1.1 nm. From estimating the NPs density at approximately 5 x 10^{10} cm^{-2}, each graphene device will present ~ 5 x 10^{8} binding sites to the biological solution. The covalent bond between gold and sulfur on the mutant M249C CRD strongly attaches the protein to the Au NPs on the graphene. These thiol bonds are commonly used in biosensing, drug delivery, and molecular biology studies for the functionalization of gold surfaces or nanoparticles (Hakkinen, 2012). The Au NPs were size selected to have an average diameter of 2.5 nm using the QMF (**Fig. S2b**), so that the protein and lactose would bind within the Debye length of the liquid gate solution. Outside of this distance, a charged molecule's electrical influence on the graphene is shielded by counterions in solution. In this work, liquid gate FET measurements were performed using a 0.01x PBS solution (pH ~ 7.4), which has a Debye length of 7.2 nm.

© 2021. This manuscript version is made available under the CC-BY-NC-ND 4.0 license
http://creativecommons.org/licenses/by-nc-nd/4.0/

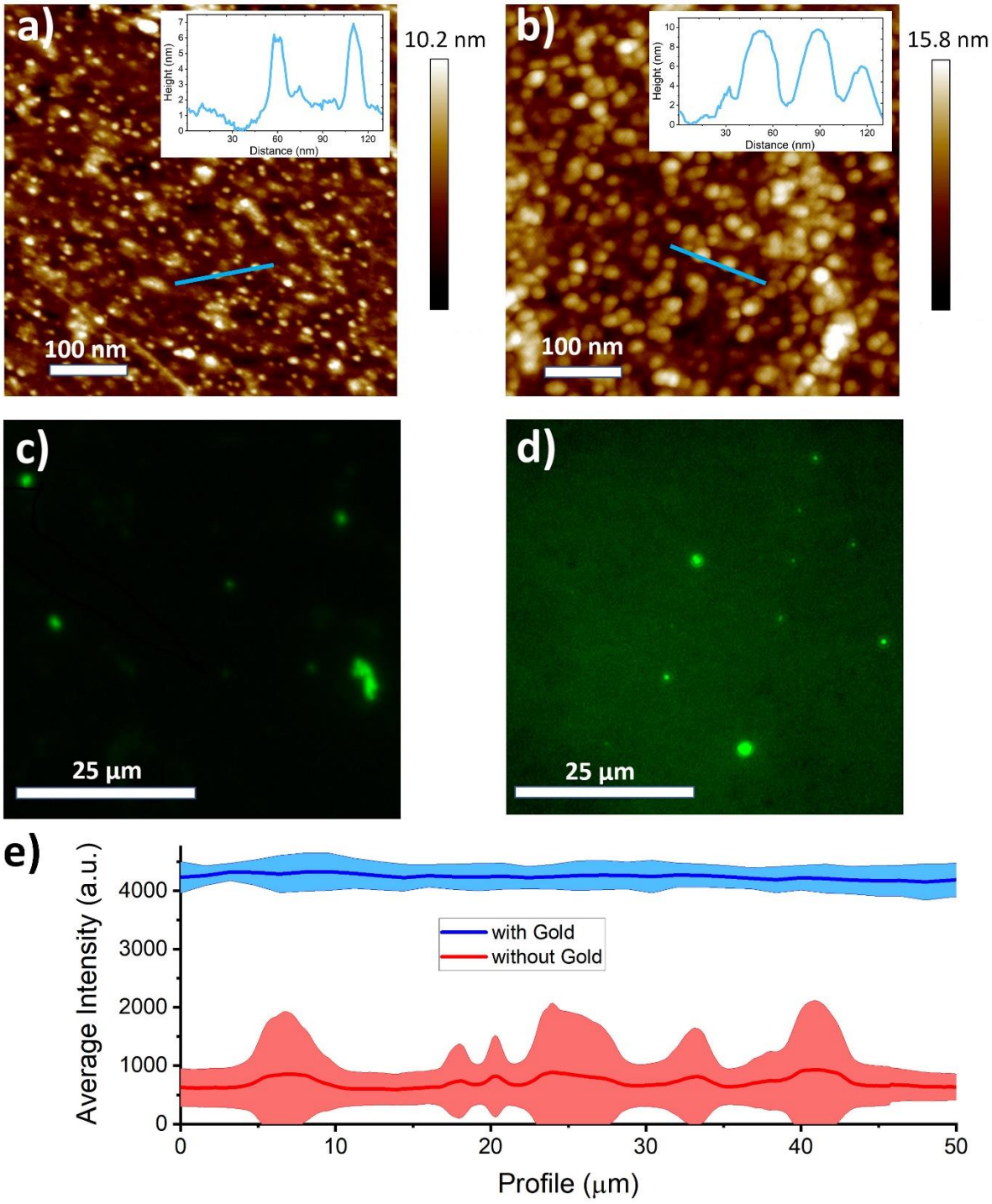

Fig. 2: Au NP – Protein Binding. AFM surface topography images of Au NP decorated graphene before **(a)** and after **(b)** immobilization of M249C hGal-3 protein. Height profiles from the indicated lines are given as insets in **(a)** and **(b)**. Fluorescent microscope images of bare **(c)** and Au NP decorated **(d)** graphene after exposure to the M249C hGal-3 protein with an Alexa Fluor 488 tag. **(e)** Average intensity from a series (n = 8) of 50 x 50 µm fluorescent microscope images of bare (bottom line) and Au NP decorated (top line) graphene after exposure to the tagged protein. Shaded areas indicate one standard deviation.

© 2021. This manuscript version is made available under the CC-BY-NC-ND 4.0 license
http://creativecommons.org/licenses/by-nc-nd/4.0/

We decided to decorate the device by reacting the lateral chain of a cysteine to the Au NP on the graphene. The only pre-existing cysteine in hGal-3 is in position 173, this position is buried in the protein structure which prevents exposure to the solvent and the possibility to react (**Fig. S4**). Taking advantage of available structural information, we planned an insertion of a cysteine in position 249. This mutation was chosen to allow the cysteine to be exposed to the solvent and free to react with the Au NP on the G-FET. Furthermore, this position is located on C-terminus of the CRD, its distance from the binding site ensures no interference with the glycan-protein interactions (**Fig. 2b**). The mutation M249C was inserted in the CRD hGal-3 by site directed mutagenesis.

As shown in **Fig. 3a**, the Far-UV spectra of the mutant M249C is comparable with that of CRD hGal-3 WT indicating that the mutation does not affect the proper folding of the protein. In addition, ITC measurements shows that the mutant M249C has a binding affinity value (K_d) for the lactose of 151 ± 17 µM (**Figs. 3b,c**), similar to the value reported for the CRD hGal-3 WT in literature (Diehl et al., 2010), confirming that the mutation does not affect the ligand binding site.

© 2021. This manuscript version is made available under the CC-BY-NC-ND 4.0 license
http://creativecommons.org/licenses/by-nc-nd/4.0/

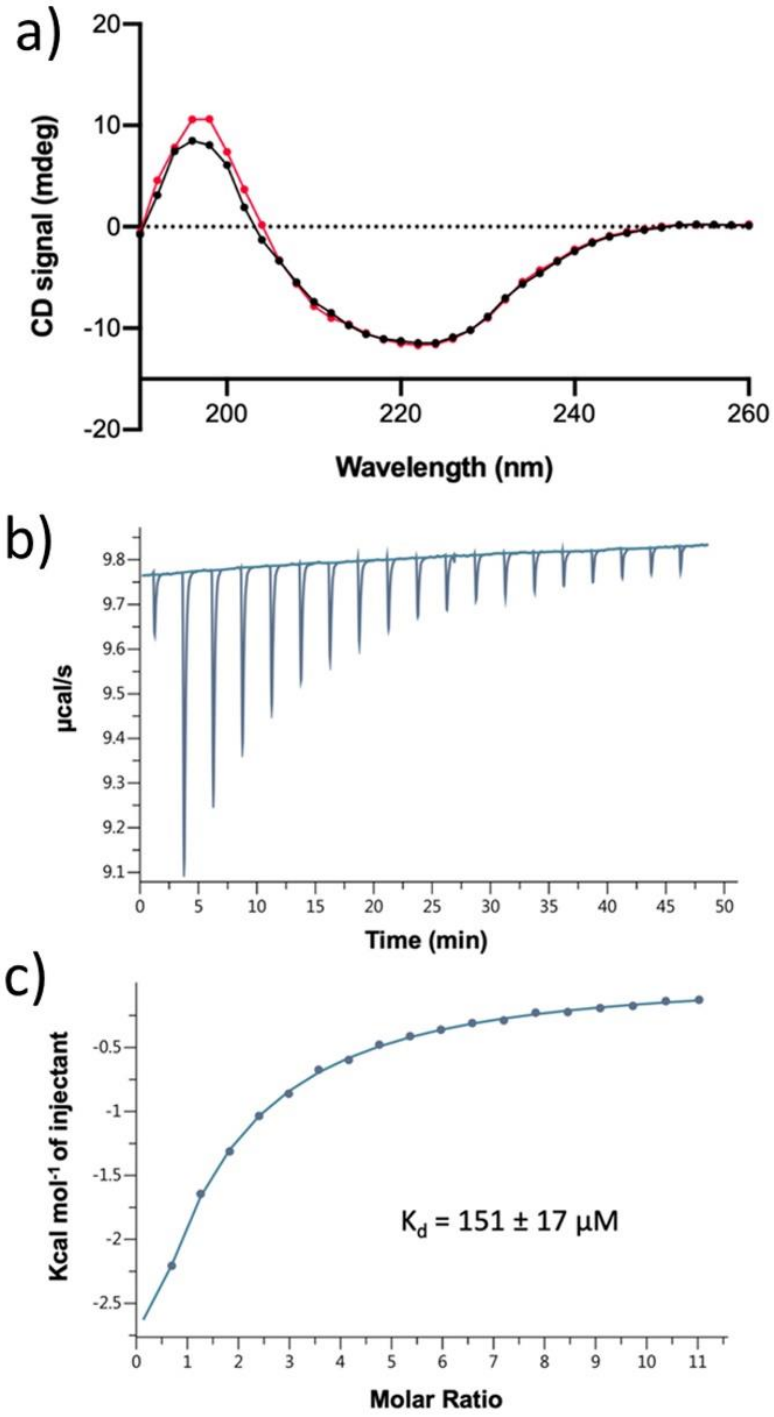

Fig. 3: CRD hGal-3 and M249C mutant characterization. (a) Far-UV CD spectra of CRD domain hGal-3 WT (black line) and the CRD hGal-3 mutant M249C (red line). The measurements were performed at 10 µM protein in water and 0.01x PBS. **(b)** ITC experimental data of the binding interaction between the CRD domain mutant M249C (30 µM) and lactose (2 mM) at 25° C. **(c)** Fitted binding curves of the extracted heats of binding as a function of added ligand for the CRD mutant M249C.

© 2021. This manuscript version is made available under the CC-BY-NC-ND 4.0 license
http://creativecommons.org/licenses/by-nc-nd/4.0/

The change in surface topography upon CRD hGal-3 M249C mutant binding was measured using AFM (**Fig. 2b**). After rinsing to remove unbound proteins, the RMS roughness of the functionalized graphene increased to ~ 2.7 nm. The increase in surface roughness and peak-to-valley height of the protein-immobilized surface can be seen in the inset surface profiles in **Fig.2a** and **2b**. Attachment of the modified protein to the graphene surface *via* the Au NP was also supported by fluorescent microscopy experiments. Both bare (**Fig. 2c**) and Au NP decorated (**Fig. 2d**) graphene sheets were exposed to a 10 µM solution of the mutant M249C CRD, labeled with the fluorescent probe Alex Fluor 488 dye. Comparing average intensities of a series of fluorescent microscope images (**Fig. 2e**), the observed fluorescence from the Au NP decorated graphene sheet is significantly higher than from the bare graphene. Some residual proteins may be bound to the bare graphene surface *via* non-specific binding to defects in the graphene, as indicated by the bright spots in **Fig. 2d**. However, these isolated areas do not approach the bound protein density of Au NP decorated graphene.

3.2 G-FET Sensor Response to Lactose

Liquid gate transfer characteristics (I_d-V_g) of the decorated G-FETs are shown in **Fig. 4a**. After decoration with Au NPs, the G-FETs initially have a V_{CNP} of approximately 0.44 V, due to p-type doping from the NP deposition and environmental adsorbates (Dong et al., 2010; Cai et al., 2015). Binding of the mutant M249C CRD causes a negative shift in V_{CNP} to ~ 0.4 V, as electron transfer from hGal-3 n-dopes the graphene (Park et al., 2011; Chen et al., 2020). Before lactose sensing, the G-FET channel is passivated with BSA to prevent non-specific binding and block reactive groups on the graphene surface (Mao et al., 2010; Yang et al., 2010).

© 2021. This manuscript version is made available under the CC-BY-NC-ND 4.0 license
http://creativecommons.org/licenses/by-nc-nd/4.0/

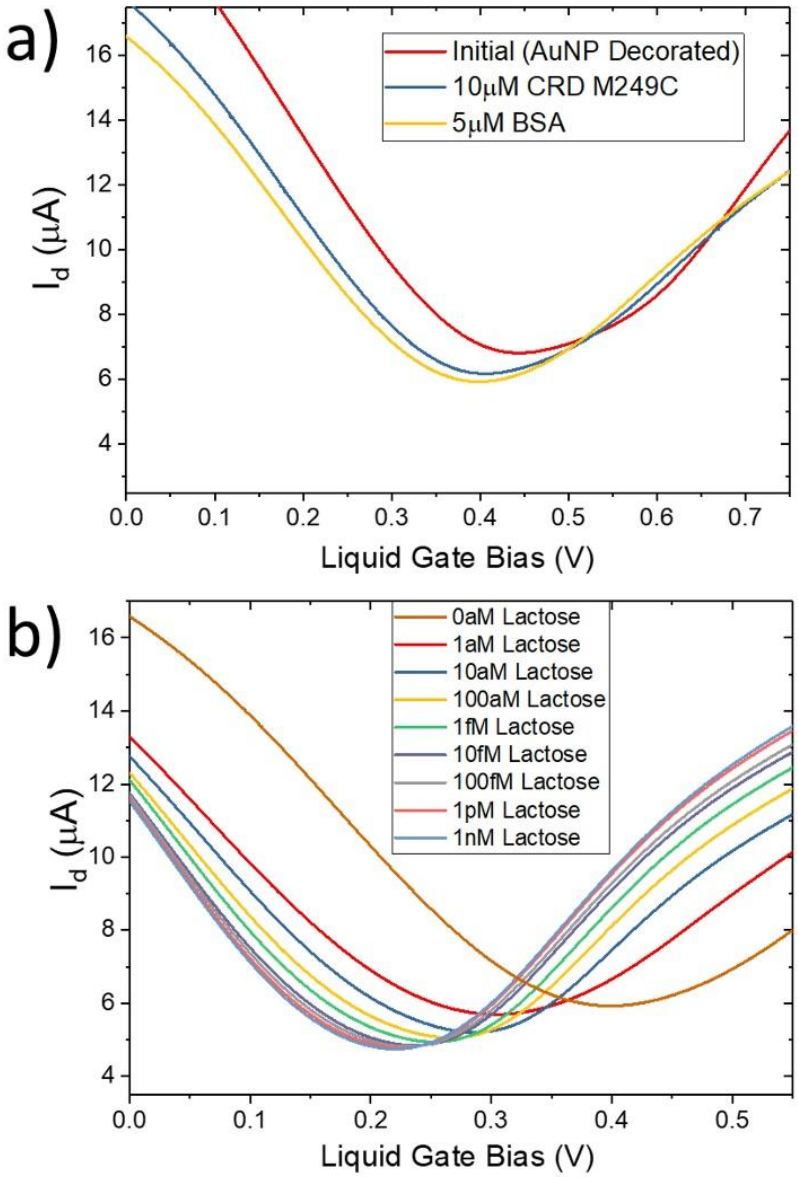

Fig. 4: G-FET Biosensor I_d-V_g Behavior. (a) Characteristic G-FET transfer curves at each functionalization step. **(b)** Characteristic G-FET transfer curves after 30 min of exposure to different concentration lactose solutions in 0.01x PBS.

The change in transfer characteristics of the G-FET in response to 0.01x PBS solutions with lactose concentrations from 1 aM to 1 nM is shown in **Fig. 4b**. Beginning with the 1 aM solution, a droplet is placed on the G-FET channel and allowed to interact with the Au NP attached mutant M249C CRD for 30 min to

© 2021. This manuscript version is made available under the CC-BY-NC-ND 4.0 license
http://creativecommons.org/licenses/by-nc-nd/4.0/

allow binding. The transfer characteristics of the device are measured using the same lactose solution in 0.01x PBS as a liquid gate, as rinsing beforehand would remove the bound lactose due to their weak H-bond attachment with the CRD. The device is rinsed using 1x PBS pH 7.4 and DI water afterwards and then exposed to a higher concentration lactose solution for 30 min before repeating the measurement. A negative shift in V_{CNP} continues with increasing lactose concentration, evidence of continued graphene n-doping as more of the attached M249C CRD binds with lactose in solution (Chen et al., 2020). At lactose concentrations greater than 10 pM, V_{CNP} saturates, as all binding sites on the graphene channel become occupied and no more doping is possible. Control experiments performed without mutant M249C conjugation or BSA passivation show the G-FET response to increasing lactose concentration in the liquid gate 0.01x PBS (**Fig. S5**); a significant positive shift in V_{CNP} that is highly unstable (± 200 mV) and exhibits no concentration dependence, as the graphene FET response is dominated by nonspecific interactions and the interface between the graphene monolayer and liquid medium, which may vary depending on the individual graphene quality and morphology. Protein-ligand binding, in contrast, dopes the graphene and adds specific binding sites such that lactose exposure produces a consistent G-FET sensor response.

3.3 Sensitivity

Fig. 5 shows the shift in the charge neutrality point (ΔV_{CNP}) with respect to lactose concentration for two series of experiments using Au NP decorated G-FETs; one with the CRD hGal-3 M249C and one with the CRD wild type (WT). The G-FET functionalized using the CRD hGal-3 M249C exhibits a log-linear response with lactose concentration between 1 fM and 1 pM before saturating at a maximum ΔV_{CNP} ~ 190 mV in the picomolar range. This corresponds to a dynamic range of 10^3, with a sensitivity of approximately 10 mV/decade. In contrast, the G-FET functionalized with the CRD Gal-3 WT exhibited a smaller absolute ΔV_{CNP} response to lactose of ~ 150 mV, which does not change with concentrations above the fM range.

© 2021. This manuscript version is made available under the CC-BY-NC-ND 4.0 license
http://creativecommons.org/licenses/by-nc-nd/4.0/

This lower response, however, was still higher than the observed ΔV_{CNP} for bare graphene (**Fig. S6**), indicating that a small amount of the CRD WT remained on the graphene. The experiment was repeated using Au NP decorated G-FETs functionalized using the CRD hGal-3 WT without His-Tag. This device's response was within the range of the bare graphene devices, indicating that the histidine residues can bind with the gold to weakly attach the CRD hGal-3 WT.

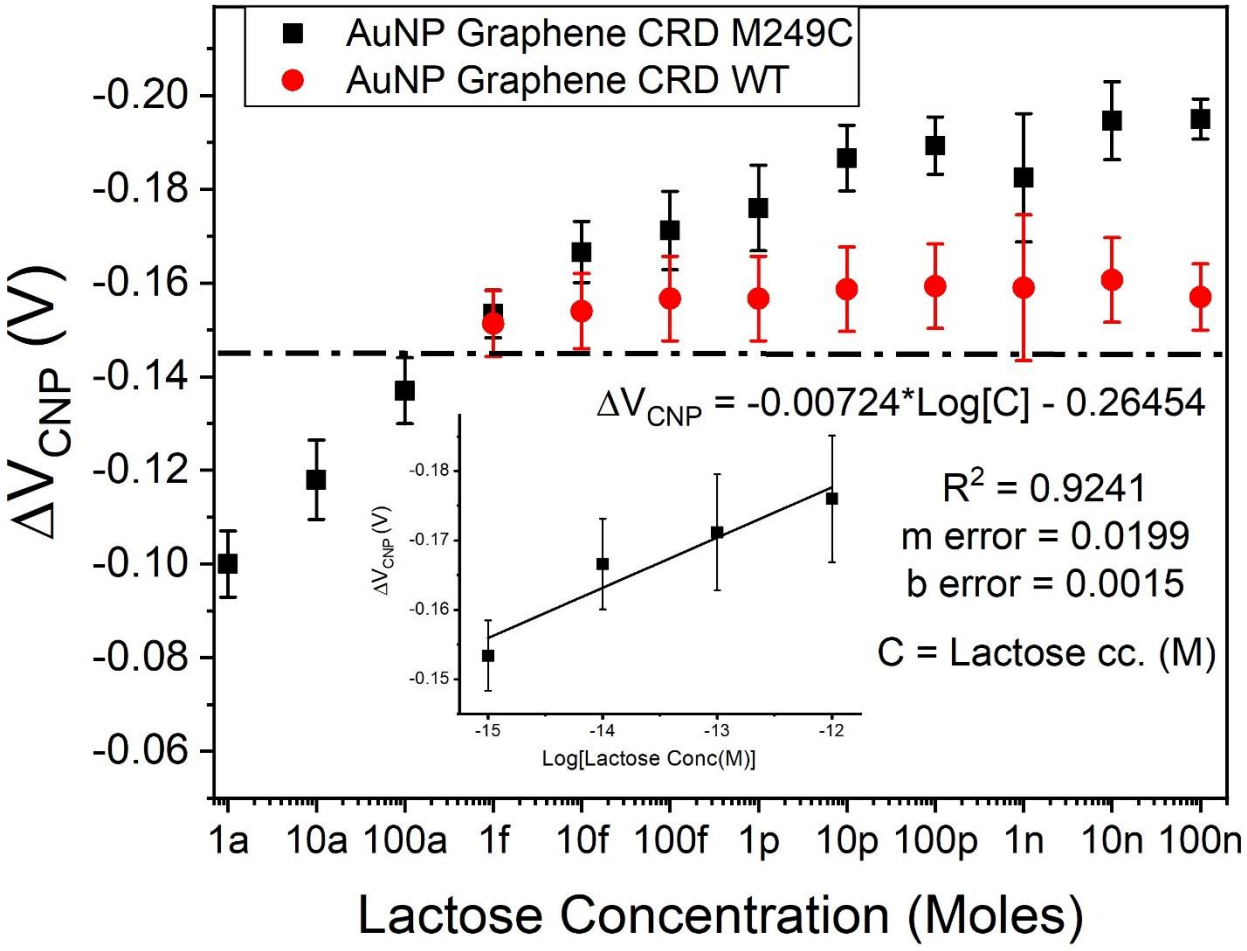

Fig. 5: G-FET Sensor Response to Lactose. The shift of V_{CNP} for Au NP decorated G-FET biosensors functionalized with the hGal-3 M249C mutant (black squares) and CRD wildtype (red circles) after exposure to lactose at concentrations from 1 aM to 100 pM. Error bars indicate standard deviations with n = 5 and the dotted line indicates the maximum response of the undecorated G-FET functionalized with CRD M249C. The inset figure illustrates the dynamic range of the sensor between 1fM and 1pM, with relevant modeling parameters.

© 2021. This manuscript version is made available under the CC-BY-NC-ND 4.0 license
http://creativecommons.org/licenses/by-nc-nd/4.0/

Control experiments using the same procedure were also performed using bare G-FETs functionalized with the mutant M249C CRD and CRD WT (**Fig. S6**). We use the maximum signal produced by the bare graphene experiments to set the limit of detection (LoD) of the sensor to ~ 200 aM, a radical improvement over many other carbohydrate sensors which present LoD in the nM to µM range (**Table S1**). From this literature survey, we see that most lactose sensors utilize an electrochemical based transduction method, catalyzed with a variety of nanomaterials (including graphene) or functionalized enzymes. We present a first demonstration of lactose detection *via* the field effect mechanism from the change in charge distribution of lectins attached to a graphene surface after lactose binding, and can compare it to other biosensor categories based on LoD, dynamic range, sensitivity, and sensing environment (Mahato et al., 2018). Our results show a clear enhancement in LoD and sensitivity in the fM range, however more work is needed to improve the robustness of the G-FET to operate in a complicated liquid environment such as diluted milk. In addition, this extremely low LoD may not be necessary in the detection of sugars which exist at high concentrations (mM) in biological fluids and food products. A more interesting application is the potential for monitoring early biosynthesis of aberrant glycans to achieve initial-stage diagnosis of a variety of cancers, such as Lewis^X, discussed in the next section.

3.4 Selectivity

To study the selectivity of the G-FET sensor, we tested the device response to solutions of glucose (one of the subunit of lactose), mannose (distinct saccharide compared to the previous tested), and sucrose (disaccharide composed of glucose and fructose) in 0.01x PBS pH 7.4 (0.1 mM) in the same manner described above. ΔV_{CNP} upon exposure to these carbohydrates at various concentrations is shown in **Fig. 6** and **Table S2**. Glucose, mannose, and sucrose all exhibit a qualitatively different ΔV_{CNP} response than

© 2021. This manuscript version is made available under the CC-BY-NC-ND 4.0 license
http://creativecommons.org/licenses/by-nc-nd/4.0/

lactose, shifting positively and indicating a p-doping of the functionalized graphene. Increasing concentrations of these carbohydrates did not significantly change ΔV_{CNP}.

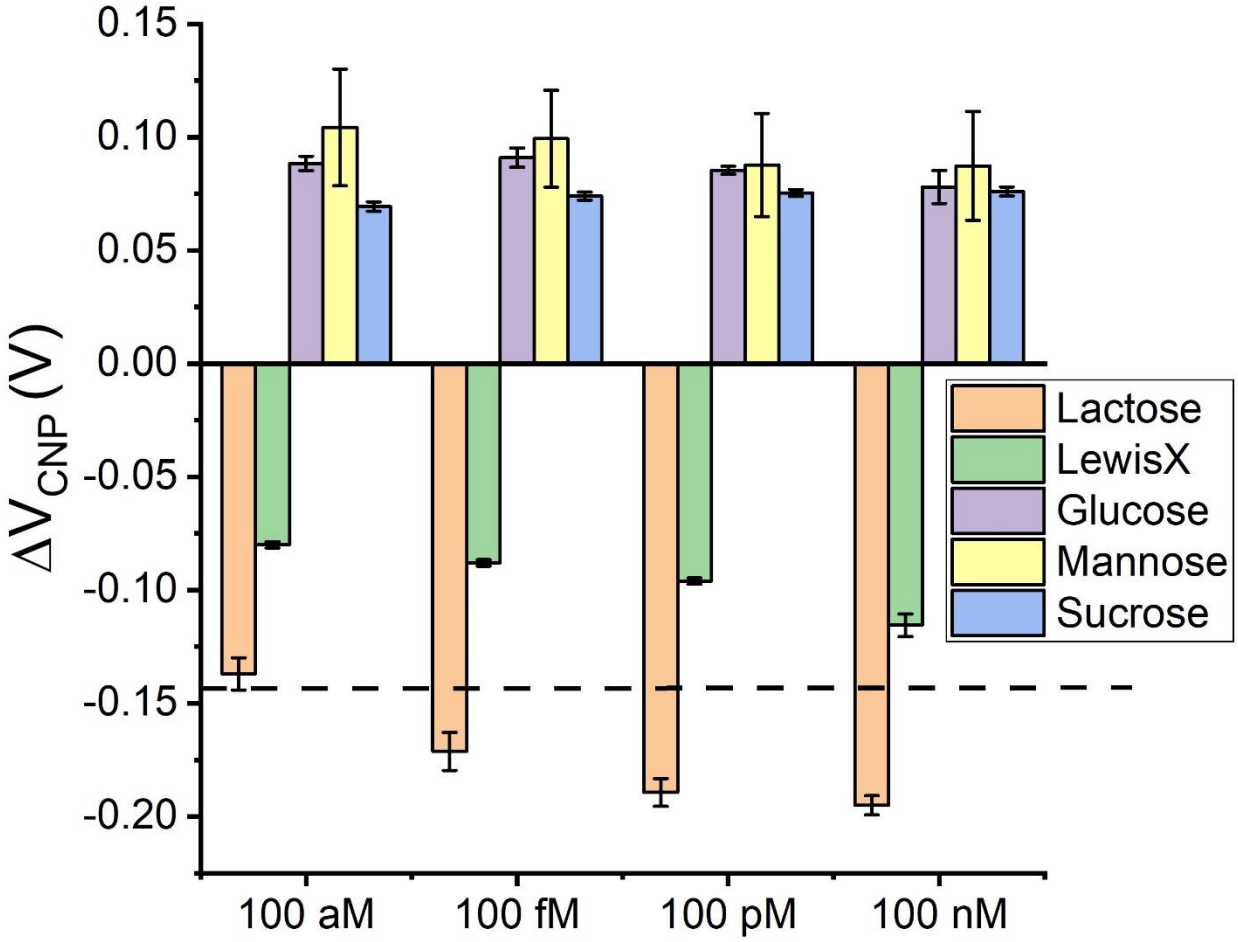

Fig. 6: G-FET Sensor Specificity. The shift of VCNP for Au NPs decorated G-FET devices after exposure to various concentrations of different carbohydrates in 0.01x PBS. Error bars indicate one standard deviation; relative standard deviation (RSD) values can be found in **Table S2**.

We also tested the G-FET sensor's response to Lewis^X, a tri-saccharide composed of fucose and N-Acetyllactosamine (**Section S5**), one of the most important blood group antigens which also plays a critical role in cell-to-cell recognition and cancer metastasis (Pérez-Garay et al., 2010; Hsieh et al., 2017). Like lactose, a negative shift in V_{CNP} was also observed in response to Lewis^X, however ΔV_{CNP} was much less than the lactose response, even at high Lewis^X concentrations. ΔV_{CNP} for different concentrations of lactose and Lewis^X are compared in **Fig. 6** and **Table S2**. Although the G-FET exhibits some sensitivity to

© 2021. This manuscript version is made available under the CC-BY-NC-ND 4.0 license
http://creativecommons.org/licenses/by-nc-nd/4.0/

Lewis^{X}, the maximum sensor response is below the noise level for an undecorated CRD-exposed G-FET (~ 145 mV negative shift).

Lewis^{X} has a much lower affinity for the mutant M249C CRD; ITC measurements with Lewis^{X} performed under the same conditions as the lactose experiments did not show any protein-ligand binding. This difference in response to the different carbohydrates illustrates the specificity of the lectin conjugated G-FET sensor to lactose. Engineering of the lectin CRD for a particular carbohydrate is necessary for the creation of a highly sensitive and specific G-FET sensor that would be clinically useful.

© 2021. This manuscript version is made available under the CC-BY-NC-ND 4.0 license
http://creativecommons.org/licenses/by-nc-nd/4.0/

4. Conclusion

In summary, we have developed a Au NP-decorated G-FET biosensor capable of label-free and ultrasensitive detection of lactose using a liquid gate measurement. The sensor is functionalized using an engineered CRD hGal-3 mutant that attaches to the Au NP-decorated graphene surface *via* a thiol bond. Affinity binding of lactose to the CRD functionalized G-FET n-dopes the graphene, causing a negative shift in the minimum voltage of the G-FET when measured in a liquid-gate configuration. This shift is specific to lactose over a 10^3 dynamic range from fM to pM levels, with an LoD of 200 aM based on control experiments using the CRD hGal-3 WT with undecorated G-FETs. Testing with other common carbohydrates produces a shift in the positive direction and does not change with analyte concentration. This device performance is a significant enhancement in sensitivity from electrochemical lactose sensors, which have been limited to the nM range. A G-FET biosensor functionalized with the appropriate lectins is a promising method to detect medically significant β-galactosides at a sub-nM level. Future work utilizing these functionalized G-FETs should focus on tailoring the lectin CRD for the desired specific carbohydrate detection.

© 2021. This manuscript version is made available under the CC-BY-NC-ND 4.0 license
http://creativecommons.org/licenses/by-nc-nd/4.0/

Acknowledgements

This work was supported by funding from the Okinawa Institute of Science and Technology Graduate University (OIST). We are grateful for the help and support provided by Dr. Alexander Badrutdinov and Dr. Hyung-Been Kang from the Engineering Support section of Research Support Division at Okinawa Institute of Science and Technology Graduate University. We thank the OIST Imaging Section for providing access to the Zeiss LSM 510 fluorescent microscope and Dr. Shinya Komoto for support. We are also grateful for data visualization help provided by Pavel Puchenkov from the Data Analysis Section of the Research Support division at OIST. We thank Prof. Hakon Leffler of Lund University for providing the hGal-3 expression gene. M.D. thanks Japan Society for the Promotion of Science (JSPS). Fellowship number: P19764

© 2021. This manuscript version is made available under the CC-BY-NC-ND 4.0 license
http://creativecommons.org/licenses/by-nc-nd/4.0/

Author Information

Corresponding Author

*Email: eric.danielson@oist.jp

Competing Interests

The authors declare no competing financial interest.

Author Contributions

Eric Danielson: Conceptualization, Methodology, Investigation, Writing – original draft, Writing - review & editing **Mirco Dindo** Methodology, Resources, Investigation, Writing – original draft, Writing - review & editing **Alexander J. Porkovich** Resources, Investigation, Writing - review & editing **Pawan Kumar** Methodology, Investigation, Writing - review & editing **Zhenwei Wang** Methodology, Investigation, Writing - review & editing **Prashant Jain** Resources, Investigation, Writing - review & editing **Trimbak Mete** Resources, Investigation **Zakaria Ziadi** Methodology, Writing - review & editing **Raghavendra Kikkeri** Conceptualization, Supervision, Project Administration **Paola Laurino** Conceptualization, Supervision, Project Administration, Writing – original draft, Writing - review & editing **Mukhles Sowwan** Conceptualization, Supervision, Project Administration

© 2021. This manuscript version is made available under the CC-BY-NC-ND 4.0 license
http://creativecommons.org/licenses/by-nc-nd/4.0/

References

Cagang, A. A., Abidi, I. H., Tyagi, A., Hu, J., Xu, F., Lu, T. J. and Luo, Z. 2016. Analytica Chimica Acta 917, 101-106.
Cai, B., Huang, L., Zhang, H., Sun, Z., Zhang, Z. and Zhang, G.-J. 2015. Biosensors and Bioelectronics 74, 329-334.
Campos, R., Borme, J., Guerreiro, J. R., Machado, G., Jr., Cerqueira, M. F., Petrovykh, D. Y. and Alpuim, P. 2019. ACS Sensors 4, 286-293.
Chen, S., Sun, Y., Xia, Y., Lv, K., Man, B. and Yang, C. 2020. Biosensors and Bioelectronics 156, 112128.
Chen, T.-Y., Loan, P. T. K., Hsu, C.-L., Lee, Y.-H., Tse-Wei Wang, J., Wei, K.-H., Lin, C.-T. and Li, L.-J. 2013. Biosensors and Bioelectronics 41, 103-109.
Collins, P. M., Hidari, K. I. P. J. and Blanchard, H. 2007. Acta Crystallographica Section D 63, 415-419.
Diehl, C., Engström, O., Delaine, T., Håkansson, M., Genheden, S., Modig, K., Leffler, H., Ryde, U., Nilsson, U. J. and Akke, M. 2010. Journal of the American Chemical Society 132, 14577-14589.
Dong, X., Shi, Y., Huang, W., Chen, P. and Li, L.-J. 2010. Advanced Materials 22, 1649-1653.
Drickamer, K. 1995. Nature Structural Biology 2, 437-439.
Fu, W., Jiang, L., van Geest, E. P., Lima, L. M. C. and Schneider, G. F. 2017. Advanced Materials 29, 1603610.
Hakkinen, H. 2012. Nature Chemistry 4, 443-455.
Hsieh, C.-C., Shyr, Y.-M., Liao, W.-Y., Chen, T.-H., Wang, S.-E., Lu, P.-C., Lin, P.-Y., Chen, Y.-B., Mao, W.-Y., Han, H.-Y., Hsiao, M., Yang, W.-B., Li, W.-S., Sher, Y.-P. and Shen, C.-N. 2017. Oncotarget 8, 7691-7709.
Justino, C. I. L., Gomes, A. R., Freitas, A. C., Duarte, A. C. and Rocha-Santos, T. A. P. 2017. TrAC Trends in Analytical Chemistry 91, 53-66.
Kiessling, L. L. and Pohl, N. L. 1996. Chemistry & Biology 3, 71-77.
Kim, D.-J., Park, H.-C., Sohn, I. Y., Jung, J.-H., Yoon, O. J., Park, J.-S., Yoon, M.-Y. and Lee, N.-E. 2013. Small 9, 3352-3360.
Lee, Y. C. and Lee, R. T. 1995. Accounts of Chemical Research 28, 321-327.
Lei, Y. M., Xiao, M. M., Li, Y. T., Xu, L., Zhang, H., Zhang, Z. Y. and Zhang, G. J. 2017. Biosensors and Bioelectronics 91, 1-7.
Liao, C., Zhang, M., Niu, L., Zheng, Z. and Yan, F. 2013. Journal of Materials Chemistry B 1, 3820-3829.
Mahato, K., Maurya, P. K. and Chandra, P. 2018. 3 Biotech 8, 149-149.
Mao, S., Lu, G., Yu, K., Bo, Z. and Chen, J. 2010. Adv Mater 22, 3521-3526.
Matsumoto, K., Maehashi, K., Ohno, Y. and Inoue, K. 2014. Journal of Physics D: Applied Physics 47, 094005.
Nguyen, B. H., Nguyen, B. T., Van Vu, H., Van Nguyen, C., Nguyen, D. T., Nguyen, L. T., Vu, T. T. and Tran, L. D. 2016. Current Applied Physics 16, 135-140.
Park, Y. K., Bold, B., Lee, W. K., Jeon, M. H., An, K. H., Jeong, S. Y. and Shim, Y. K. 2011. International Journal of Molecular Sciences 12.
Peña-Bahamonde, J., Nguyen, H. N., Fanourakis, S. K. and Rodrigues, D. F. 2018. Journal of Nanobiotechnology 16, 75.
Pérez-Garay, M., Arteta, B., Pagès, L., de Llorens, R., de Bolòs, C., Vidal-Vanaclocha, F. and Peracaula, R. 2010. PLOS ONE 5, e12524.
Porkovich, A. J., Ziadi, Z., Kumar, P., Kioseoglou, J., Jian, N., Weng, L., Steinhauer, S., Vernieres, J., Grammatikopoulos, P. and Sowwan, M. 2019. ACS Nano 13, 12425-12437.
Saraboji, K., Hakansson, M., Genheden, S., Diehl, C., Qvist, J., Weininger, U., Nilsson, U. J., Leffler, H., Ryde, U., Akke, M. and Logan, D. T. 2012. Biochemistry 51, 296-306.

© 2021. This manuscript version is made available under the CC-BY-NC-ND 4.0 license
http://creativecommons.org/licenses/by-nc-nd/4.0/

Shivayogimath, A., Whelan, P. R., Mackenzie, D. M. A., Luo, B., Huang, D., Luo, D., Wang, M., Gammelgaard, L., Shi, H., Ruoff, R. S., Bøggild, P. and Booth, T. J. 2019. Chemistry of Materials 31, 2328-2336.
Suvarnaphaet, P. and Pechprasarn, S. 2017. Sensors 17.
Varki, A., Cummings, R. D., Esko, J. D., Stanley, P., Hart, G. W., Aebi, M., Darvill, A. G., Kinoshita, T., Packer, N. H., Prestegard, J. H., Schnaar, R. L. and Seeberger, P. H. (2017). Essentials of Glycobiology. Woodbury, NY, Cold Spring Harbor Laboratory Press.
Viswanathan, S., Narayanan, T. N., Aran, K., Fink, K. D., Paredes, J., Ajayan, P. M., Filipek, S., Miszta, P., Tekin, H. C., Inci, F., Demirci, U., Li, P., Bolotin, K. I., Liepmann, D. and Renugopalakrishanan, V. 2015. Materials Today 18, 513-522.
Yang, M. and Gong, S. 2010. Chemical Communications 46, 5796-5798.
Zhao, S., Liu, Z., Chen, P., Sun, J. and Shen, X. 2019. Journal of Electroanalytical Chemistry 845, 106-110.

© 2021. This manuscript version is made available under the CC-BY-NC-ND 4.0 license
http://creativecommons.org/licenses/by-nc-nd/4.0/